Cathodoluminescence of near-surface centres in Cr-doped MgO(001) thin films probed by scanning tunnelling microscopy

2012 New J. Phys. 14 033006

(http://iopscience.iop.org/1367-2630/14/3/033006)

New Journal of Physics
The open-access journal for physics

Cathodoluminescence of near-surface centres in Cr-doped MgO(001) thin films probed by scanning tunnelling microscopy

Fernando Stavale, Niklas Nilius[1] and Hans-Joachim Freund
Fritz-Haber-Institut der Max-Planck-Gesellschaft, Faradayweg 4–6, D-14195 Berlin, Germany
E-mail: nilius@fhi-berlin.mpg.de

New Journal of Physics **14** (2012) 033006 (14pp)
Received 7 December 2011
Published 6 March 2012
Online at http://www.njp.org/
doi:10.1088/1367-2630/14/3/033006

Abstract. Crystalline MgO films with a defined level of Cr dopants (MgO_{Cr}) are prepared by either subsequent or simultaneous deposition of Cr and Mg atoms in an oxygen ambience onto a Mo(001) support. The structural and morphological parameters of the doped films are investigated using low-energy electron diffraction and scanning tunnelling microscopy (STM). Whereas at low Cr concentration the doped oxide has similar properties to pristine MgO(001), a new Cr/Mg mixed oxide develops at higher Cr load. The nature of the Cr impurities in the MgO matrix is deduced from cathodoluminescence spectroscopy performed by electron injection from the STM tip into the oxide film. In agreement with earlier studies on MgO_{Cr} bulk crystals, the majority of Cr adopts a 3+ charge state and occupies Mg substitutional sites. The dopants give rise to sharp emission lines at about 700 nm, arising from radiative electron transitions between the Cr 3d levels split in the MgO crystal field. From the spectral evolution upon annealing the MgO_{Cr} films, we deduce a strong tendency of the dopants to accumulate in a near-surface region. Our experiments demonstrate that high-quality MgO_{Cr} films with similar optical properties as bulk samples can be prepared on conductive supports, being a first step to make doped oxide materials accessible to surface science studies.

[1] Author to whom any correspondence should be addressed.

Contents

1. Introduction

The elucidation of the optical properties of transition-metal impurities in wide-gap insulators is closely connected with the MgO_{Cr} model system [1]. By using MgO single crystals doped with Cr in the sub-percent range, the fundamental mechanisms of light absorption and emission have been related to d–d transitions in individual Cr^{3+} centres sitting in Mg^{2+} substitutional sites. The main emission line at 698 nm arises from magnetic-dipole transitions between the ^2E and ^4A irreducible representation of the Cr^{3+} ions in a cubic environment [2]. Additional lines are produced by Cr^{3+} in non-centrosymmetric sites, being adjacent to defects or the oxide surface [3]. The main lines are accompanied by sidebands at higher wavelengths that reflect the presence of phonon-mediated emission processes [4]. The assignment of the various optical transitions relies on calculations of the local crystal field in conjunction with the dipole selection rules and has been confirmed by electron paramagnetic resonance (EPR) spectroscopy [5].

Whereas MgO_{Cr} single crystals are ideally suited for optical measurements thanks to the large number of optically active centres and the perfect long-range order, they are irrelevant for surface-science studies due to their electrically insulting nature. Consequently, neither imaging techniques with atomic resolution capabilities, e.g. electron or scanning tunnelling microscopy (STM), nor electron spectroscopy have been used so far to characterize the position and charge state of the Cr ions in the MgO host. A thorough investigation of doped oxide materials is, however, mandatory when not optical but chemical properties are in the focus of research. Doped oxides form the basis for various applications in material sciences, chemical sensing and heterogeneous catalysis [6–8]. In the latter case, the ability of the dopants to exchange electrons with adsorbates on the oxide surface is of particular interest, as this may constitute the initial step for a chemical reaction. For example, oxygen radicals produced by Li^+ dopants in MgO are expected to activate gas-phase methane [9, 10], while transition-metal impurities are involved in various oxidation and hydrogenation reactions [11]. As shown in a recent study, Mo dopants in a CaO matrix are able to alter the equilibrium shape and charge state of metal deposits and hence key parameters of supported metal catalysts [12]. Experiments along this line always require finite conductivity of the oxide system and cannot be performed on single crystals.

The main goal of this study was to prepare MgO_{Cr} films that are thin enough to enable conventional surface-science studies, but still exhibit the characteristic optical response of bulk MgO_{Cr} crystals [13]. The latter is important, because the optical signature contains information on the charge state and local environment of the dopants that is not accessible otherwise. The main challenge was the implementation of an optical method that is sensitive enough to probe Cr dopants in MgO films of 10–20 monolayers (ML) thickness, which is the critical value for the electrical conductivity to break down [14]. We will show that cathodoluminescence spectroscopy performed with an STM is the method of choice, as it enables the simultaneous structural and optical characterization of the sample surface. Electron injection from the tip produces optical excitations in the oxide film that can be probed with a sensitive photon detector in the far field. Moreover, the signal can be monitored with high spatial resolution, limited only by the diameter of the exciting electron beam. By this means, ensembles of a few hundreds of Cr dopants can be investigated, which strongly reduces the impact of statistical disorder and inhomogeneous broadening. Still, the optical response is fully compatible with the results from MgO_{Cr} bulk crystals where more than 10^{20} centres contribute to the signal. Our approach even allows us to identify Cr^{3+} ions in a near-surface region that are subject to a different electron–phonon coupling and crystal field than their bulk counterparts.

2. Experiment

The measurements were made in an ultrahigh vacuum (UHV) chamber (2×10^{-10} mbar) equipped with a liquid-nitrogen-cooled STM, as well as standard tools for sample preparation and analysis. The STM setup was specifically designed to detect photons emitted from the tip–sample junction [15]. For this purpose, a Beetle-type head is placed inside a parabolic mirror with the tip being in the focal point. The mirror collects light from a large solid angle and reflects it out of the UHV chamber. A second parabolic mirror focuses the light onto the entrance slit of the grating spectrograph (150 lines mm^{-1}) coupled to a CCD detector. The optical setup allows us to probe very low photon fluxes in the wavelength range 200–1200 nm.

Pristine MgO films of 15 ML thickness were prepared by Mg vapour deposition in 5×10^{-7} mbar O_2 onto a well-prepared Mo(001) single crystal at room temperature [16–18]. The initially amorphous films were annealed to 1100 K for 10 min to stimulate their crystallization. The resulting surface revealed a (1×1) square pattern in low-energy electron diffraction (LEED). The cross-shaped spot profiles thereby indicated a slight mosaicity of the film, arising from the 5% lattice mismatch between MgO and the Mo(001) support [18]. STM images exhibited wide, atomically flat oxide terraces, being approximately 100 nm^2 in size and delimited by a network of dislocation lines (figure 1(a)). The dislocations are remnants of the original oxide grains that merged into a closed film upon annealing, but also facilitate the internal strain compensation in the film. The Cr was dosed onto the surface either after or during film preparation, using an e-beam evaporator. The atom flux was calibrated with a quartz microbalance and by dosing Cr onto bare Mo(001), where the Cr-covered surface fraction could be readily determined with the STM.

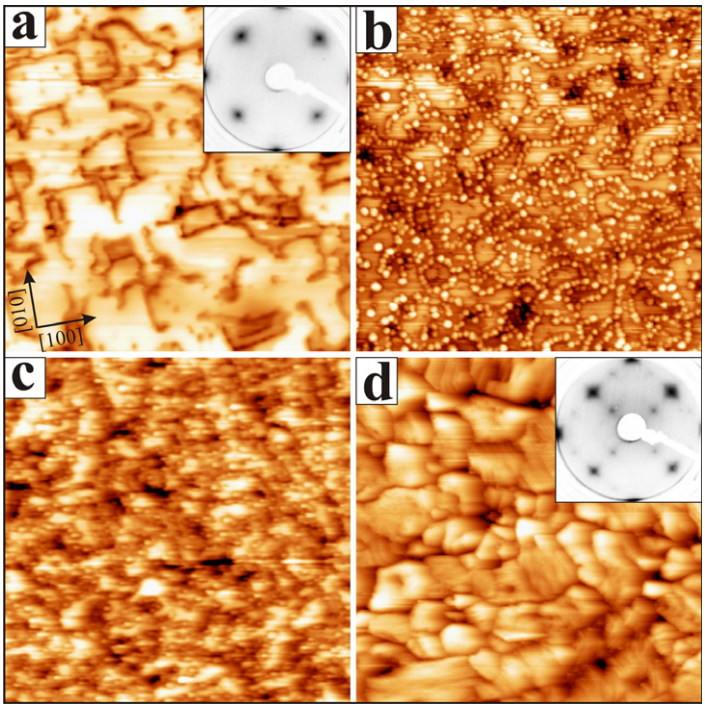

Figure 1. (a) STM topographic image and LEED pattern taken at 55 eV of a pristine 15 ML thick MgO film. (b) The same surface after dosing 0.5 ML of Cr at room temperature and (c) after annealing to 750 K (3.5 V, $120 \times 120\,\mathrm{nm}^2$). (d) STM image and LEED pattern of a mixed oxide, prepared by depositing 3 ML of Cr onto 15 ML of MgO and annealing to 800 K in 5×10^{-7} mbar O_2 (6.5 V, $350 \times 350\,\mathrm{nm}^2$). The mixed phase is characterized by a granular morphology and a (2×1) LEED pattern (55 eV electron energy).

3. Results and discussion

3.1. Preparation and morphology of Cr-doped MgO films

Two techniques have been developed to produce crystalline MgO films doped with small Cr quantities. The first one starts off with Cr deposition on top of a 15 ML thick MgO/Mo film that is annealed afterwards to stimulate Cr diffusion into the surface. Figure 1(b) displays a typical starting configuration with 0.5 ML Cr dosed onto the surface. The metal preferentially nucleates at MgO line defects, producing linear assemblies of small aggregates with roughly 1.6 nm diameter. This nucleation preference reflects the enhanced binding potential of chemically unsaturated defect sites, as analysed in detail in earlier studies [19, 20]. Only 15% of the Cr deposits are found on the oxide terraces, where the mean particle diameter is somewhat larger (2.5 nm). With increasing Cr exposure, new particles nucleate on the oxide terraces, while deposits along the defect lines only grow in size. Heating such ensembles at 800 K in UHV causes the mean particle diameter to shrink, while their density remains constant due to an effective pinning to the oxide defects (figure 1(c)). The decrease in particle volume is assigned to two effects. Whereas part of the Cr sublimates into the gas phase, a smaller fraction penetrates the oxide film using the MgO dislocation lines as the diffusion channel. At temperatures beyond

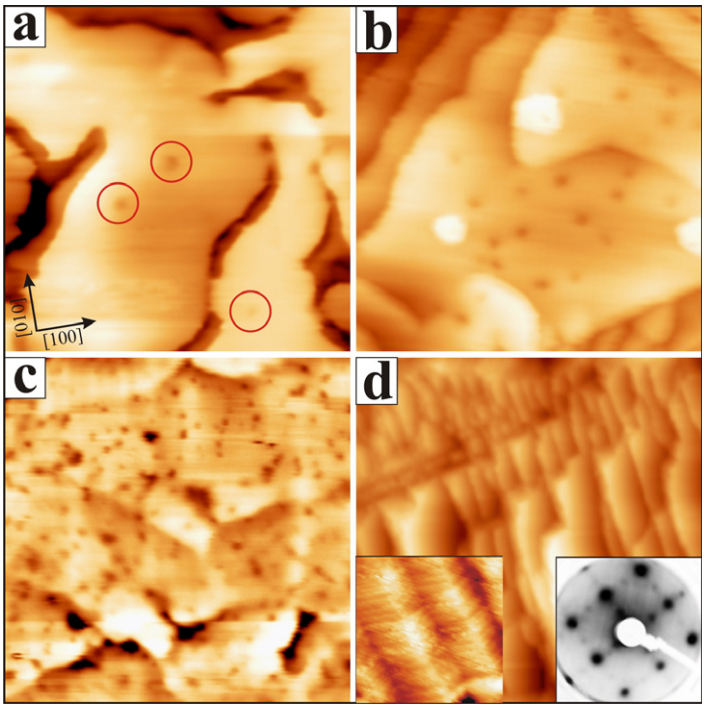

Figure 2. STM topographic images of Cr/Mg mixed oxides on Mo(001) after annealing to 1000 K ($35 \times 35\,nm^2$, 1.5 V). The Cr concentration rises from (a) 0.05%, (b) 0.5% to (c) 1%, producing an increasing number of atom-sized holes in the surfaces. (d) Mixed Cr/Mg oxides with 10% dopant concentration ($200 \times 200\,nm^2$, −6.5 V). The insets show a single roof-like grain ($25 \times 25\,nm^2$) and the LEED pattern of the corresponding sample.

1000 K, the Cr aggregates completely disappear from the surface, but without recovering the initial MgO surface morphology. In fact, the film now exposes a characteristic granular structure with typical grains of 20–50 nm diameter and 2–3 nm height (figure 1(d)). This morphology change is accompanied by the occurrence of a new LEED pattern, which displays a faint (2×1) superstructure in addition to the fundamental (1×1) MgO spots. We note that the surface restructuring becomes more pronounced at higher Cr loads and if the annealing step is performed in 5×10^{-7} mbar O_2. We will show later that both the new morphology and the (2×1) LEED pattern reflect the formation of a Cr/Mg mixed oxide on top of the MgO(001).

The main drawback of producing doped MgO samples via inter-diffusion is the inhomogeneous distribution of Cr inside the film and its accumulation at the surface. A more regular distribution is achieved by inserting the dopants directly during oxide growth. To explore this route, we have exposed a clean Mo surface simultaneously to a constant Mg and a variable Cr flux in 5×10^{-7} mbar O_2 followed by an annealing step in UHV. The resulting surface morphologies, measured as a function of Cr concentration, are shown in figure 2. For dopant levels below 0.1 at.%, pristine and doped MgO exhibits the same surface topography regarding terrace size and film smoothness. A small number of atom-sized depressions is detected on top of the films ($<5 \times 10^{11}\,cm^{-2}$), which increases to $\sim 5 \times 10^{12}$ and $\sim 2 \times 10^{13}\,cm^{-2}$ with the Cr concentration rising to 0.5 to 1%, respectively (figures 2(b) and (c)). Still, the MgO rocksalt structure is maintained for light doping and the sample exhibits the characteristic (1×1) LEED

pattern. The surface constitution changes, however, for Cr concentrations above 5%, when the granular morphology appears again in STM and a (2×1) LEED pattern with two orthogonal domains becomes visible in LEED (figure 2(d)). The observed grain size in this case depends on the initial Cr load, reaching about 20 nm for 10% nominal Cr concentration. Apparently, the same surface morphology is obtained when annealing either a Cr/MgO ad-system or a mixed MgO_{Cr} film if only the initial doping level is sufficiently high.

3.2. Optical characterization of Cr-doped MgO films

Further information on the MgO systems doped via one or the other approach is obtained from cathodoluminescence spectroscopy, using the known emission response of bulk MgO_{Cr} as a reference [1, 3]. Photoluminescence, a more common technique, is not applicable to the 15 ML films used here due to the low number of active centres and the opaque nature of the Mo substrate. The cathodoluminescence spectra were taken by electron injection from the negatively biased STM tip at ∼100 nm distance from the surface into a pre-selected sample region. The electron energy was varied between 50 and 300 eV. Whereas below 200 eV, long detection times were required to obtain spectra with a good signal-to-noise ratio, large numbers of defects were created in the surface at higher energy, most likely due to electron-induced desorption of oxygen [21]. As a compromise between emission cross section and surface damage, we acquired most of the spectra with 200 eV excitation energy. Still, photon accumulation times of 300 s and large spectrometer slit widths had to be used to account for the low photon fluxes, limiting the spectral resolution to about $\Delta\lambda = 10$ nm.

Figure 3(a) shows three cathodoluminescence spectra taken on a pristine MgO film (top), after exposure to 0.5 ML Cr (middle) and after annealing to 1000 K in UHV (bottom). The topmost spectrum is characterized by a broad emission band at 410 nm, originating from the radiative recombination of MgO excitons at threefold coordinated oxygen ions [22, 23]. The relevant exciton traps are located along the dislocation network of the MgO films, as proven by the quenching of the characteristic light emission via depositing small amounts of gold that also nucleate on the line defects [24]. Similarly, the MgO emission disappears after Cr dosage, because the exciton recombination centres become covered as well. However, whereas the Au deposits generate a strong plasmonic excitation on their own, Cr-covered MgO films are optically inactive [25]. The photon signal reappears after annealing such samples to 1000 K, when a faint emission line emerges at ∼700 nm. According to the STM, most of the Cr evaporates during this treatment while a small part penetrates the film, as suggested by the 700 nm emission peak that matches the optical fingerprint of bulk MgO_{Cr} [1]. The new band gains in intensity if more Cr is loaded onto the surface and the annealing is performed in O_2 (figure 3(a), bottom curve). Samples prepared in this way are characterized by a granular surface morphology and a (2×1) LEED pattern, as shown in figure 1(d). We note that the 410 nm emission peak does not reappear upon annealing, because the exciton recombination sites remain blocked by Cr remnants.

Mixed MgO_{Cr} films, prepared by Cr and Mg co-deposition in an O_2 atmosphere, display a similar optical response. Already at low Cr concentration (0.05%), a small shoulder at 700 nm appears next to the broad exciton-mediated emission band at 410 nm (figure 3(b), top). At this dopant level, statistically only 500 Cr centres are probed by the impinging electron beam. With increasing concentration, the MgO emission quickly fades away, proving the site-blocking effect to be active again, while the Cr-related signal gains in intensity. Starting from 1% doping

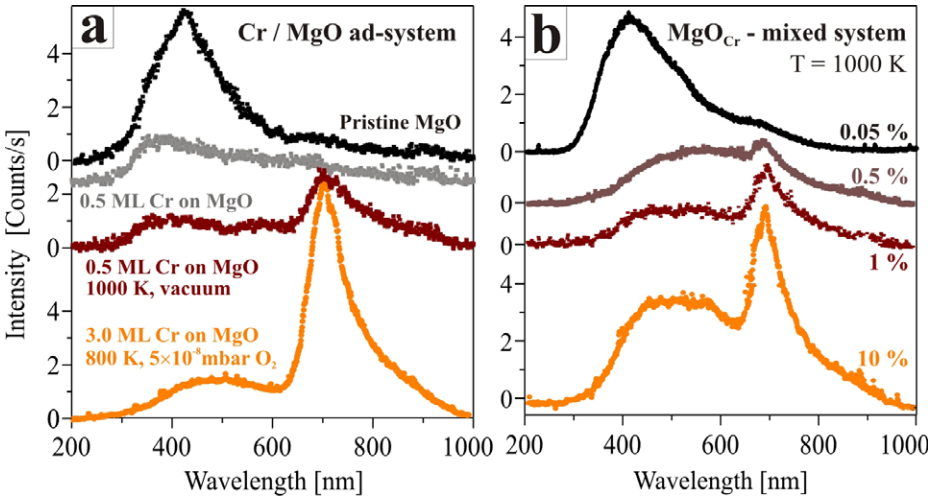

Figure 3. (a) Cathodoluminescence spectra measured on a pristine 15 ML thick MgO film, an MgO film covered with 0.5 ML Cr and the same film after annealing to 1000 K (from the top). The bottom spectrum has been taken after annealing 3 ML Cr on 15 ML MgO in oxygen at 800 K. (b) Similar spectra measured for 15 ML MgO films homogeneously doped with the given Cr amounts. All spectra have been taken with 200 eV electron energy, 5 nA current, 300 s integration time and 1 mm slit width of the monochromator.

level (around 10 000 Cr centres in the beam), spectral fine structure appears and the 700 nm band splits into two pronounced maxima at 698 and 717 nm and a few kinks that are not resolved by our grating spectrograph[2]. Below 10% Cr content, the spectral shape remains essentially constant despite the massive surface restructuring observed in the STM (figure 2(d)). The intensity course can still be disentangled into two main bands at 698 and 717 nm and a third broad peak at 820 nm. With even higher Cr loading, the 700 nm emission fades away, reflecting the development of a thick and ill-defined chromium oxide layer on top of the MgO film.

The optical response of mixed MgO_{Cr} films has additionally been probed for different film preparations, in particular for different annealing temperatures. Such a spectral series is shown in figure 4(a) for a 15 ML thick film doped with 1% Cr. This doping level was chosen as it guarantees the integrity of the MgO rocksalt lattice while maximizing the emission yield. Both the total intensity and the ratio between the two main bands at 698 and 717 nm were found to change with temperature. At 800 K, which is the onset temperature for crystallization, the integral emission is low and both bands appear with similar intensity. At higher temperature, mainly the high-wavelength band increases until it dominates the spectrum for films annealed to 1100 K. We will show later that this spectral evolution is compatible with the accumulation of Cr at the MgO surface. Further insight into the nature of Cr-induced light emission is gained from experiments performed at two different film thicknesses, 15 and 100 ML (doping level 1%) (figure 4(b)). The latter sample could no longer be imaged with STM due to the low conductivity,

[2] The experimental peak positions are generally red-shifted by 5–8 nm due to the linear Stark effect induced by a tip electric field of approximately 1×10^9 V m^{-1}.

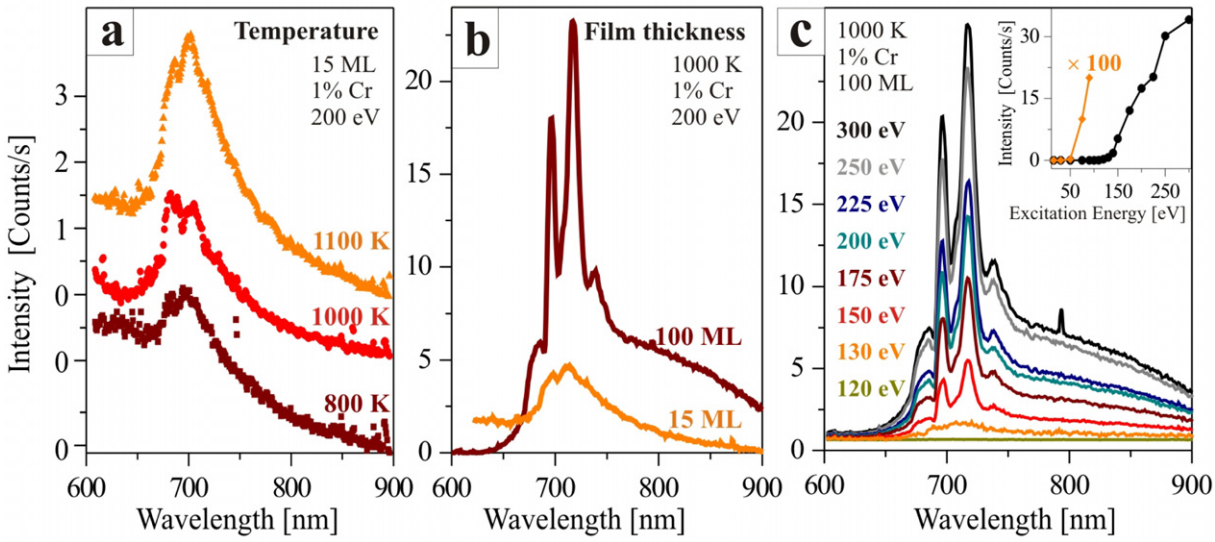

Figure 4. Cathodoluminescence spectra of MgO thin films doped with 1% Cr, measured as a function of the annealing temperature (a), the film thickness (b) and the energy of the exciting electrons (c). The inset shows the increase of emission yield with electron energy. Whereas spectra on 15 ML films have been measured with 1 mm slit width, 0.1 mm slits have been used for the 100 ML films (5 nA electron current). The widths of the main emission lines at 698 and 717 nm are still governed by the diffractive power of our spectrograph.

but displayed the characteristic MgO(001) LEED pattern. The emission yield was found to be ten times larger for 100 ML than for 10 ML thick films, which is explained by the higher number of Cr centres and their superior decoupling from the Mo support that offers effective non-radiative decay channels. The intense emission from thick films allowed us to improve the spectral resolution by reducing the monochromator slit width to 0.1 mm. However, even those settings were insufficient for resolving the fine structure of the main bands at 698 and 717 nm, and only two additional features were detected at 683 and 707 nm. In a final experiment, we have explored the dependence of the 700 nm emission lines on the kinetic energy of the incoming electrons (figure 4(c)). The threshold energy that produced a detectable photon flux at 5 nA current was determined to be 50–70 eV, depending on the quality and sharpness of the STM tip. With increasing energy, the photon signal rises exponentially but flattens out above 200 eV. The monotonic intensity course is interrupted by a step at ∼250 eV, at which the intensity nearly doubles. We note that similar excitation behaviour has been found for excitons in bare MgO(001) films before.

3.3. Discussion: structural aspects

For the sake of clarity, we analyse the structure and morphology of MgO films with homogeneous Cr distribution (mixed films) first and discuss the ad-systems that feature Cr enrichment at the surface thereafter. Both LEED and STM measurements indicate a weak perturbation of the MgO rocksalt structure at Cr levels in the sub-percent range. The most obvious doping effect is the occurrence of atom-sized holes on the surface, which start appearing at 0.1%

Cr load and evolve to the most abundant defect type above 1% Cr concentration (figure 2). Those features are assigned either to Cr impurities that have segregated to the surface upon annealing or to Mg vacancies that are known to be present in MgO_{Cr} [1, 26]. The vacancies form in the oxide lattice to compensate for the charge difference between the Cr^{3+} dopants and the substituted Mg^{2+} ions. According to EPR and optical measurements, the missing electron cannot be stabilized in the high-spin Cr system, as the hosting orbital already overlaps with the MgO conduction band [2]. To avoid the presence of high-energy electrons, trap states are produced in the band gap by introducing Mg defects into the oxide lattice. Each vacancy creates two low-lying hole states in adjacent O ions that are filled with excess electrons of two Cr^{3+} donors. The concept of mutual interactions between the Mg vacancies and the Cr centres has been successfully used to describe the optical and spin spectra measured on MgO_{Cr} bulk samples, providing solid evidence for the anticipated Cr^{3+} charge state [27].

An unambiguous assignment of the hole features observed in the STM to either Cr impurities or Mg vacancies is difficult at this point. We favour the second option, because the defects appear as plain depression in the accessible bias range, while foreign species should exhibit a bias-dependent contrast due to the availability of new electronic states for tunnelling [28, 29]. Moreover, the formal positive charge of the Cr^{3+} ion would induce a local downward bending of the MgO bands, which increases the accessible state density at positive sample bias and gives rise to protruding features, in contrast to the experimental findings [30]. We therefore suspect that the observed defects are indeed Mg vacancies that have segregated to the surface upon annealing. The efficiency of this process can be estimated by comparing the initial Cr load with the number of voids in the surface (figure 2). For 1% Cr concentration, 2×10^{13} surface defects are found per cm^2, which accounts for $\sim$25% of the required vacancies to achieve charge neutrality in the MgO film. We note that vacancy accumulation on the surface has been identified for Li-doped MgO films before, with the difference that O and not Mg defects are created in that case due to the undervalent nature of Li [31].

The segregation process described above also promotes Cr enrichment in a near-surface region of MgO. If a critical dopant level is reached, the Cr ions can no longer be incorporated into the rocksalt lattice and a new Cr/Mg mixed oxide develops on the surface. The thermodynamically most stable composition of the three elements is $MgCr_2O_4$ (magnesium chromate), with Cr^{3+} and Mg^{2+} ions sitting in octahedral and tetrahedral positions of a cubic O^{2-} lattice, respectively [32]. The growth of this phase is supported by the (2×1) LEED pattern observed for Cr-rich samples, as the $MgCr_2O_4$ lattice parameter is nearly twice as large as that of MgO(001) (0.83 nm versus 0.42 nm). The residual strain might prevent good epitaxial growth along both the MgO⟨100⟩ directions and no (2×2) registry is detected. Such a unidirectional growth of the chromate is also in line with the STM data that show regular stripes in one MgO direction but a dense step pattern in the other (figure 2(d)). This grain morphology might be explained as $MgCr_2O_4$ sheets stacked along one MgO⟨100⟩ direction. Due to the fourfold symmetry of the MgO lattice, two orientations are possible in accordance with the two (2×1) domains seen in LEED. Our $MgCr_2O_4$ structure model can only be tentative and needs to be confirmed by additional experimental techniques, e.g. grazing-incidence x-ray diffraction. A similar mixed oxide seems to develop upon annealing a Cr particle ensemble to more than 800 K in O_2, as shown in figure 1(d). In this case, the critical Cr/Mg ratio for chromate formation is reached via Cr diffusion into and Mg diffusion out of the MgO support. The similarity of both phases despite different preparation procedures underlines the energetic preference of $MgCr_2O_4$ with respect to other Cr/Mg/O compounds.

3.4. Discussion: optical properties

Weakly doped MgO_{Cr} single crystals have been intensively studied with both absorption and emission spectroscopy, providing a solid basis for the interpretation of our thin-film data [1, 3, 33]. The most intense emission is usually the R line at 698 nm that relates to $^2E \rightarrow {}^4A_2$ transitions in Cr^{3+} ions placed at Mg^{2+} substitutional sites with octahedral symmetry [2]. Additional bands appear for dopants in low-symmetry lattice positions, i.e. next to a Mg vacancy, where the initial ^2E state gets split and the emission moves to higher wavelength (N lines at 699–703 nm). Another broad peak is detected at ∼800 nm that originates from $^4T_2 \rightarrow {}^4A_2$ transitions in the Cr *d* manifold and only shows up if the $^4T_2$ level shifts below the ^2E as expected for Cr^{3+}–Mg vacancy pairs aligned with a MgO[110] direction [34]. Both the R and N lines are accompanied by vibronic sidebands, i.e. the original line is downshifted by the energy of a typical MgO phonon [4]. Several of those bulk MgO_{Cr} transitions are indeed identified in the emission spectra of our thin films. At low Cr concentrations (0.5%), only a single broad photon peak is resolved at 700 nm, covering the wavelength region of the R and N lines and their respective sidebands (figure 3, upper spectra). Due to the low emission yield of weakly doped films and the need to work with large spectrometer slit widths, no fine structure is resolved in this case. Starting from 1% doping level, the 700 nm peak can be disentangled into several bands that are best resolved for the highly luminescent 100 ML thick films (figure 4(b)). The most intense peaks at 698 and 717 nm are assigned to a convolution of the zero-phonon R and N bands and their respective phonon sidebands. We note that a tenfold larger diffraction power would be necessary to separate these bands with our spectrometer. The slow decay of the photon intensity beyond 740 nm indicates the presence of another peak at higher wavelength, which can be fitted with a Gaussian of 100 nm width and 820 nm central wavelength. Given the limited spectral resolution, this peak is in reasonable agreement with the emission characteristic of [110]-oriented Cr^{3+}–Mg vacancy pairs in bulk MgO_{Cr} samples.

The overall spectral shape does not change for Cr concentrations beyond 1%; however, the fine structure in the 700 nm region becomes more complex and an assignment of the optical transitions more difficult (figure 3, lower spectra). We take the spectral complexity as an indication for the increasing inhomogeneity of our samples with more Cr^{3+} ions occupying low-coordinated sites adjacent to Mg vacancies and the surface. The associated symmetry reduction modifies the local crystal field acting on the Cr 3d states, but also alters the dipole selection rules and therewith the visibility of certain transitions. In addition, exchange coupling between adjacent Cr centres becomes a relevant parameter at high dopant concentrations [35]. Even if $MgCr_2O_4$ grains start growing on the surface at 5% Cr level, the spectral response remains unchanged. This finding might be explained by a similar local environment of the Cr^{3+} in doped MgO and the chromate phase, as the ions occupy octahedral sites in the cubic O lattice in both cases. In fact, the emission properties of Cr^{3+} in various compounds, such as ruby, emerald and alexandrite, were found to be similar despite pronounced structural differences [36]. Moreover, the emission signature of the $MgCr_2O_4$ grains cannot be separated from the signal of isolated Cr species in the MgO, as both elements always coexist in our samples. We therefore refrain from a detailed interpretation of the emission spectra obtained for Cr-rich samples and just emphasize that the general emission course is similar for systems produced by annealing a Cr ad-layer or embedding Cr into an MgO film (figure 3).

Focusing on lightly doped films again, one immediately realizes the high intensity of the phonon sideband at 717 nm with respect to the zero-phonon line. In photoluminescence spectra

obtained on bulk MgO_{Cr}, the zero-phonon line is typically four times stronger than the phonon line due to the small Huang–Rhys parameter of MgO_{Cr}, which compares to a ratio of 0.75 in our case [1]. We ascribe this intensity boost of the phonon sidebands to two effects. First, the electrons in cathodoluminescence spectroscopy interact vigorously with the oxide ions and effectively excite lattice phonons [37]. Radiative recombination therefore takes place in a vibrationally highly excited system, giving rise to intense phonon lines. The importance of inelastic interactions between impinging electrons and MgO phonons is supported by the experimental result that the intensity ratio between zero-phonon and phonon lines declines with increasing energy, i.e. the phonon contribution becomes stronger at higher excitation energies (figure 4(c)). The second reason concerns the position of the dopants inside the film. We expect the Cr ions and associated Mg defects to accumulate in a near-surface region, where the vacancy formation energy is lower and the structural flexibility of the MgO lattice is higher [31]. Recombination processes in near-surface Cr^{3+} species are particularly affected by interactions with the lattice phonons. On the one hand, the surface phonons are softer and produce larger spatial displacements of the ions [38, 39]. This leads to a temporary lowering of the cubic symmetry of Cr^{3+} centres, which releases the dipole selection rules and increases the phonon-mediated emission cross section. On the other hand, electron–phonon coupling is known to be larger at the MgO(001) surface compared to the bulk [40], which again intensifies the phonon contribution. A local heating of the MgO under the electron beam, as an alternative explanation for the strong phonon sidebands, is discarded here because of the low dissipated power ($<1\,\mu$W) and the good thermal contact between MgO films and Mo support [41]. Assuming the sample to be bulk MgO, we estimate the local heating to be below 50 K under the given experimental conditions.

An indirect proof for the close interrelation between strong phonon sidebands and Cr accumulation on the surface comes from annealing experiments as shown in figure 4(a). When heating a 1%-doped MgO film from 800 to 1100 K, the total emission increases, but more importantly the phonon sideband gains in intensity. Whereas the first effect reflects the improved crystallinity and the absence of non-radiative decay channels in well-annealed films, the second one arises from the segregation of Cr species to the surface. As pointed out earlier, near-surface dopants are subject to much stronger phonon-assisted emission processes than bulk species sitting in a perfect octahedral environment [37]. We note that this interpretation is fully supported by STM images taken during the annealing series, which also reveals an increasing density of atom-sized depressions on the surface.

In the last section of this work, we want to address the excitation mechanism for MgO_{Cr} luminescence via electron impingement (figure 4(c)). Strikingly, no emission is detected at electron energies below 50 eV, although all relevant Cr d transitions occur below 3 eV energy. We suspect that direct energy transfer from the incoming electrons to the Cr electronic system is inefficient, most likely because of the dipole-forbidden nature of transitions inside the d-state manifold. At higher initial energy, a multitude of indirect excitations become accessible, e.g. electron–hole-pair excitations in the MgO host, Auger transitions in the Cr^{3+} and the MgO, as well as impact ionization [42]. For example, the ionization thresholds for the Mg 2s, p, the O 2s and the Cr 3p levels are all about 50 eV. Moreover, each incoming projectile produces a cascade of secondary electrons that are able to interact with the Cr centres as well. On the other hand, not every excited Cr centre with an electron in high crystal-field states necessarily emits a photon, as non-radiative recombination channels such as multi-phonon emission and Landau damping via the Mo support are also available. It is the sum of all those effects that renders

a low-energy stimulation of the Cr dopants impossible and puts the threshold energy for light emission to ~ 50 eV. We cannot decide at this point whether this threshold is intrinsic to the decisive excitation step in the MgO_{Cr} system (e.g. the creation of a deep hole) or due to the insufficient detection sensitivity of our optical setup.

Beyond the threshold, the emission intensity rises exponentially first but flattens out at higher energy. The exponential increase is compatible with the excitation cross section of many intermediate steps, e.g. the creation of secondary electrons and electron–hole pairs by the incoming projectiles. In addition, the tip–sample distance, and hence the excitation volume, increases with electron energy, moving more and more Cr species into the beam. The subsequent flattening of the emission rise indicates a lower excitation probability at higher energy, as expected once the electron free-mean path exceeds the film thickness [43]. Above 100 eV injection energy, also a degradation of the MgO film, e.g. due to oxygen desorption, can no longer be excluded. The pronounced step in the energy-dependent emission yield at 250 eV has not been analysed in detail so far. No Auger or ionization thresholds are available in the Mg, O or Cr ions at this energy; however, the ionization threshold of the Mo 3d states is about 250 eV. The involvement of the Mo support, e.g. via secondary electrons that temporarily occupy the Cr electronic system, might therefore explain the pronounced step in the excitation cross section. An experimental proof for this scenario, for instance by probing the emission yield as a function of the MgO film thickness, is, however, beyond the scope of this paper.

4. Conclusion

By means of STM, LEED and cathodoluminescence spectroscopy, we have demonstrated that well-defined MgO_{Cr} films can be grown on a Mo(001) single crystal. In weakly doped films, the presence of surface Mg vacancies that balance the Cr^{3+} charge state with respect to the substituted Mg^{2+} ions is the sole morphological fingerprint for Cr incorporation. At higher Cr load, a granular structure becomes visible in the STM, being ascribed to a new $MgCr_2O_4$ phase that forms on the MgO surface. In contrast to structure-sensitive approaches, the doping effect is evident in light emission spectra of the MgO_{Cr} system. In good agreement with earlier studies on doped bulk crystals, the Cr centres introduce several photon bands between 698 and 820 nm. Our STM-based optical technique allows us to detect these dipole-forbidden and hence notoriously weak optical transitions in oxide films of 15–100 ML thickness. Furthermore, distinguishing between Cr ions in the sub-surface and bulk regions of the film becomes possible due to the different phonon contributions in both cases. So far, stimulation of the photon emission has been feasible only for relatively high electron energies, which is responsible for the low spatial resolution of our method. This drawback might be overcome in future by combining optical and electronic excitations of the dopants and would enable us to characterize small ensembles or even single Cr ions in the MgO host. By this means, the optical response of impurity ions might be connected with their position inside the MgO lattice, providing useful information on the local distribution and charge state of dopants in oxide films.

Acknowledgments

FS thanks the Alexander v Humboldt Stiftung for financial support. The authors acknowledge support from the DFG within the Cluster of Excellence UniCat.

References

[1] Henderson B and Imbusch G F 1989 *Optical Spectroscopy of Inorganic Solids* (Oxford: Clarendon)
[2] Tanabe Y and Sugano S 1954 *J. Phys. Soc. Japan* **9** 753
[3] Larkin J P, Imbusch G F and Dravnieks F 1973 *Phys. Rev.* B **7** 495
Henry M O, Larkin J P and Imbusch G F 1976 *Phys. Rev.* B **13** 1893
O'Neill M B and Henderson B 1988 *J. Lumin.* **39** 161
[4] Sangster M J L 1972 *Phys. Rev.* B **6** 258
[5] Wertz J E and Auzins P 1957 *Phys. Rev.* **106** 484
Griffiths J H E and Orton J W 1959 *Proc. Phys. Soc.* **73** 948
[6] Shapovalov V and Metiu H 2007 *J. Catal.* **245** 205
Ganesh R, Pala S and Metiu H 2007 *J. Phys. Chem.* C **111** 12715
[7] Rodriguez J A, Hanson J C, Kim J Y, Liu G, Iglesias-Juez A and Fernandez-Garcia M 2003 *J. Phys. Chem.* B **107** 3535
Nambu A, Graciani J, Rodriguez J A, Wu Q, Fujita E and Sanz J F 2006 *J. Chem. Phys.* **125** 094706
[8] Tanaka H, Tan I, Uenishi M, Kimura M and Dohmae K 2001 *Top. Catal.* **16/17** 63
Tanaka H, Taniguchi M, Kajita N, Uenishi M, Tan I, Sato N, Narita K and Kimura M 2004 *Top. Catal.* **30/31** 389
[9] Wang J X and Lunsford J H 1986 *J. Phys. Chem.* **90** 5883
Ito T, Wang J X, Lin C H and Lunsford J H 1985 *J. Am. Chem. Soc.* **107** 5062
[10] Lunsford H 1995 *Angew Chem., Int. Ed. Engl.* **34** 970
[11] Pala R G S and Metiu H 2007 *J. Phys. Chem.* C **111** 12715
Nolan M, Verdugo V S and Metiu H 2008 *Surf. Sci.* **602** 2734
[12] Shao X, Prada S, Giordano L, Pacchioni G, Nilius N and Freund H-J 2011 *Angew Chem., Int. Ed. Engl.* **50** 11525
[13] Kantorovich L N, Shluger A L and Stoneham A M 2001 *Phys. Rev.* B **63** 184111
[14] Nilius N 2009 *Surf. Sci. Rep.* **64** 595
[15] Freund H-J, Nilius N, Risse T, Schauermann S and Schmidt T 2011 *Chem. Phys. Chem.* **12** 79
[16] Gallagher M C, Fyfileds M S, Cowin J P and Joyce S A 1995 *Surf. Sci.* **339** L909
[17] Valeri S, Altieri S, del Pennino U, di Bona A, Luches P and Rota A 2002 *Phys. Rev.* B **65** 245410
Schintke S and Schneider W D 2004 *J. Phys.: Condens. Matter* **16** R49
[18] Benedetti S, Benia H M, Nilius N, Valeri S and Freund H-J 2006 *Chem. Phys. Lett.* **430** 330
Benedetti S, Torelli P, Valeri S, Benia H M, Nilius N and Renaud G 2008 *Phys. Rev.* B **78** 195411
[19] Neyman K M, Inntam C, Matveev A V, Nasluzov V A and Rosch N 2005 *J. Am. Chem. Soc.* **127** 11652
[20] Benedetti S, Myrach P, di Bona A, Valeri S, Nilius N and Freund H-J 2011 *Phys. Rev.* B **83** 125423
[21] Kramer J, Tegenkamp C and Pfnür H 2003 *Phys. Rev.* B **67** 235401
[22] Anpo M, Yamada Y, Kubokawa Y, Coluccia S, Zecchina A and Che M 1988 *J. Chem. Soc. Faraday Trans.* **84** 751
[23] Stankic S, Muller M, Diwald O, Sterrer M, Knözinger E and Bernardi J 2005 *Angew. Chem., Int. Ed. Engl.* **44** 4917
Stankic S, Diwald O, Bernardi J and Knözinger E 2006 *J. Phys. Chem.* B **110** 13866
[24] Benia H M, Myrach P and Nilius N 2008 *New J. Phys.* **10** 013010
Benia H M, Lin X, Gao H J, Nilius N and Freund H-J 2007 *J. Phys. Chem.* C **111** 10528
[25] Kreibig U and Vollmer W 1995 *Optical Properties of Metal Clusters (Springer Series Materials Science* vol 25) (Berlin: Springer)
[26] Zheng W C and Wu S Y 1996 *J. Phys.: Condens. Matter* **8** 4539
[27] Carroll J C G, Corish J, Henderson B and Mackrodt W C 1988 *J. Mater. Sci.* **23** 2824
[28] Nörenberg H and Harding J H 1999 *Appl. Surf. Sci.* **142** 174
Batzill M, Katsiev K, Gaspar D J and Diebold U 2002 *Phys. Rev.* B **66** 235401

[29] Bechstein R, Kitta M, Schütte J, Kühnle A and Onishi H 2009 *J. Phys. Chem.* C **113** 3277
[30] Nilius N, Ganduglia-Pirovano V M, Brazdova V, Kulawik M, Sauer J and Freund H-J 2010 *Phys. Rev.* B **81** 045422
[31] Myrach P *et al* 2010 *ChemCatChem* **2** 854
[32] O'Neill H S C and Dollase W A 1994 *Phys. Chem. Miner.* **20** 541
[33] Imbusch G F, Schawlow A L, May A D and Sugano S 1965 *Phys. Rev.* A **140** 830
[34] Castelli F and Forster L S 1975 *Phys. Rev.* B **11** 920
[35] Schawlow A L, Wood D L and Clogston A M 1959 *Phys. Rev. Lett.* **3** 271
[36] Gaft M, Reisfeld R and Panczer G 2005 *Luminescence Spectroscopy of Minerals and Materials* (Berlin: Springer)
[37] Glass A M 1967 *J. Chem. Phys.* **46** 2080
Fernández I and Llopis J 1988 *Phys. Status Solidi* a **108** K163
[38] Savio L, Celasco E, Vattuone L and Rocca M 2003 *Phys. Rev.* B **67** 075420
[39] Nelin C J, Bagus P S, Brown M A, Sterrer M and Freund H-J 2011 *Angew Chem., Int. Ed. Engl.* **50** 10174
[40] Fujimori A and Tsuda N 1988 *Surf. Sci. Lett.* **100** L445
[41] Pignatel G U and Queirolo G 1983 *Radiat. Eff.* **79** 291
Mason R A 1994 *Chem. Geo.* **111** 245
[42] Kramer J, Ernst W, Tegenkamp C and Pfnür H 2002 *Surf. Sci.* **517** 87
Kramer J, Tegenkamp C and Pfnür H 2003 *Phys. Rev.* B **67** 235401
[43] Akkerman A, Boutbou T, Breskin A, Chechik R, Gibrekhterman A and Lifshitz Y 1996 *Phys. Status Solidi* b **198** 769